05,10

Low-temperature dielectric and magnetic properties of composite brass nanoparticles obtained at an electron accelerator by electron beam evaporation from a two-zone crucible

© D.A. Smolyakov[1], E.V. Eremin[1,2], M.S. Molokeev[1], K.V. Zobov[3], M.N. Volochaev[1], A.S. Tarasov[1]

[1] Kirensky Institute of Physics, Federal Research Center KSC SB, Russian Academy of Sciences, Krasnoyarsk, Russia
[2] Siberian State University of Science and Technology, Krasnoyarsk, Russia
[3] Khristianovich Institute of Theoretical and Applied Mechanics, Siberian Branch, Russian Academy of Sciences, Novosibirsk, Russia

E-mail: sda88@iph.krasn.ru

Received September 21, 2023
Revised September 21, 2023
Accepted November 8, 2023

In this paper presents the results of a study of Cu/Zn composite brass nanoparticles obtained from a two-zone crucible using an electron accelerator for target irradiation. Characterization was carried out, the chemical and phase composition of the manufactured samples was determined using transmission electron microscopy, energy-dispersive X-ray spectroscopy and X-ray diffraction analysis. The dielectric properties of the nanopowder have been studied. Features of the relaxation type were discovered. The energy of the activation process is estimated. The magnetic properties of the sample demonstrate a paramagnetic character, which was expected due to the composition of the nanopowder. However, against the background of the paramagnetic contribution, there is a ferromagnetic phase, which is clearly visible at low temperatures and practically disappears at room temperature. This indicates that some part of the composite nanoparticles have long-range magnetic order at low temperatures.

Keywords: Nanoparticles, nanopowders, composite, electron accelerator, dielectric properties, paramagnets.

DOI: 10.61011/PSS.2024.01.57859.209

1. Introduction

Current technological challenges in various research and production applications require the use of a wide range of new materials and improvement of their synthesis methods. These are new materials that form the basis of one of the advanced research areas — nanotechnology. Besides nanoscale structures such as thin films, nanotubes and nanowires, nanoparticles and nanopowders play an important role in this area [1]. The latter are powders with particle sizes up to 100 nm. One of the important properties of the powder nanoparticles is in the increased surface area [2]. This allows them to be used as catalysts and catalyst or absorbent carriers. Nanoscale particles may render new properties to materials, which is attractive in terms of production development. For example, composite manufacturing using nanopowders makes it possible to achieve their mechanical properties [3]. Moreover, these materials may be also used for environmental applications for removal of heavy metals pollution [4].

Nanopowders may be used as potential replacement of the existing materials in manufacturing of various structures. Thus, copper nanoparticles may be treated as an alternative to precious metals. This provides wide opportunities for application in electronics, magnetic and optical devices, catalysts and pigments. It is also interesting that copper nanoparticle properties depend to a great extent on their synthesis methods. [5]. Interest in copper oxides is also high, because they are used in solar cells, have high solar absorption, low heat radiation, nontoxicity and simple production process [6]. Copper oxides are known as *p*-type semiconductors. For example, films produced by the photoelectrochemical reduction demonstrate typical semiconductor behavior [7]. Also, CuO shows multiferroic properties at temperatures below 230 K [8], which is interesting in terms of possible applications. For nanoscale materials, electrical and optical properties may be much different from bulk properties. As to polycrystals, the role of surface states increases with a decrease in grain sizes, thus, also influencing the magnetic properties of low-dimensional CuO. [9]. Focus is also made on another well known ZnO semiconductor [10]. Having a wide band gap (3.37 eV), this low-cost semiconductor with controlled conductivity may be widely used in solar cells [11] and gas detectors [12]. Therefore, interest in zinc and copper composite nanoparticles — brass nanoparticles, is also high. Structures based on nanoscale brass particles have good prospects of nanoelectronics applications [13]. Moreover, the brass particles have also high antibacterial properties [14].

There is currently a wide range of nanoparticle production methods. However, preference is given to methods combining high productivity, environmental friendliness and high

end product yield. Such methods may include production of nanoparticles by the gas-phase synthesis method using high-power electron emission source. This method using an electron accelerator makes it possible to perform the processes that do not occur or flow very slowly in normal conditions. By changing the process variables, nanoparticles with the pre-defined shape, morphology and chemical analysis may be produced.

It can be inferred that nanoparticles are of much interest with researchers. Nanopowder production, investigation and implementation activities in various modern research and technology areas are very important. Herein, focus is made on the characterization of the copper/zinc composite nanopowder produced using the electron accelerator by the electron-beam evaporation, and on the measurement of its dielectric and magnetic properties.

2. Synthesis and characterization of samples

Cu/Zn composite nanoparticle samples were prepared by the electron-beam treatment of a brass/copper target placed into a two-zone crucible (Figure 1).

Industrial relativistic electron beam accelerator with energy of 1.4 MeV and current in the range of 5–25 mA was used as a material heater. Grade M0 copper is placed in the center of the graphite crucible, grade L63 brass is placed on the periphery. A 14 kW electron beam from the accelerator irradiates copper which melts and evaporates emitting a part of heat through the graphite crucible wall to the brass ingot. On the periphery, brass achieves the alloy melting temperature sufficient for intense zinc evaporation from molten brass. Metal vapors are carried over by argon and deposited in the form of nanoparticles in a box filter [15].

The synthesized samples were characterized. Transmission electron microscopy (TEM) was performed. Figure 2 shows ball-shaped granules of different sizes and needle-shaped nanoparticles. Copper nanoparticles are ball-shaped, rod-shaped and plate-like particles are typical for zinc nanostructures. It could be noted that the sample has particles of various sizes (from 2 to 200 nm). Mean dimension of the powder nanoparticles was calculated from

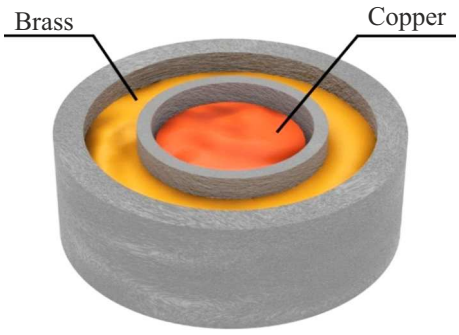

Figure 1. Schematic representation of a two-zone crucible.

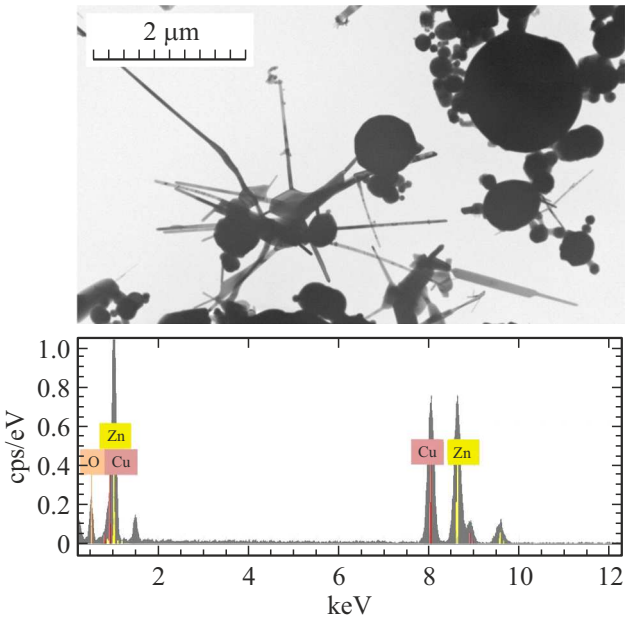

Figure 2. TEM image of the test sample and EDS spectrum of elements contained in the nanopowder.

the specific surface measurements. To the approximation of the same size and spherical shape of all particles, correlation between the specific surface S and mean particle size d is known:

$$S = 4\pi R^2/\rho\,\frac{4}{3}\pi R^3 = 6/\rho d, \qquad (1)$$

where ρ is the brass density equal to $8.5 \cdot 10^3$ kg/m^3, $S = 5.6$ m^2/g. Thus, a mean particle size of $d = 126$ nm may be calculated. Taking into account the microscopy data and chemical inhomogeneity of the compound, the prepared powders may be assigned to nanoscale powders.

Then, to determine the powder composition and the presence of impurities, chemical analysis was conducted on the prepared samples by the energy-dispersive X-ray spectroscopy (EDS) (Figure 2). EDS spectrum is well fit by Cu, Zn and O lines which is indicative of the prevailing concentration of these elements in the powder and minor concentration of additional impurities.

X-ray diffraction analysis of the sample was also conducted. Powder diffraction data for the Rietveld analysis were acquired at room temperature using Haoyuan DX-2700BH powder diffractometer with CuK_α radiation and linear detector. Increment 2θ was 0.01°, counting time was 0.2 s per increment. Almost all peaks were indexed by several phases: Cu, Zn, Cu_2O ZnO, CuZn and $Cu_{1-x}Zn_x$. Therefore, these structures were assumed as a starting model for refinement by the Rietveld method which was performed using TOPAS 4.2 software [16]. Atom positions and thermal parameters of all phases or refinement were fixed due to large peak overlap and high correlation of these parameters. The refinements were stable and gave low R-factors: $R_{wp} = 10.12\%$, $R_p = 7.79\%$ (Figure 3).

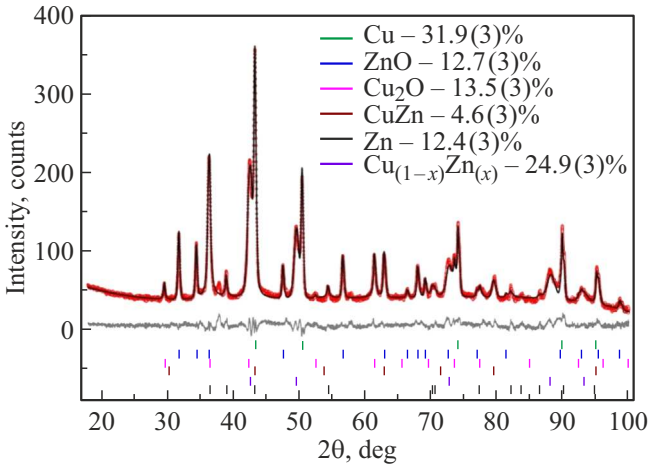

Figure 3. Differential Rietveld plot with percentage of main phases.

The acquired data suggests that the expected Cu/Zn composite constitutes about 30% of the total powder weight. The powder contains Cu and Zn particles as well as Cu and Zn oxides. Generally, it can be suggested that the result is satisfactory, although the preparation technique is new and has not been finalized completely.

3. Experimental findings and discussion

After characterization of the material, dielectric parameters were measured. For this, the test sample was placed in a tailor-made measurement cell (Figure 4). This is a plate-parallel capacitor with two copper plates. The plate diameter was 10 mm, the distance between them was 1 mm. Nanopowder was poured between the plates and tightly pressed. The measurements were conducted on a special-purpose test unit for testing transport and magnetotransport properties of bulk materials and nanomaterials [17–19] in alternating current in a wide temperature range from 5 to 270 K. Capacity properties were recorded using Agilent E4980A LCR-meter running at current frequencies from 20 Hz to 2 MHz. Temperature dependences of capacity $C(T)$ and loss-angle tangent $\mathrm{tg}\,\delta(T)$ at different frequencies in heating mode with 5 K. Using dependences $C(T)$, real and imaginary dielectric permittivity components were derived.

Dielectric permittivity may be estimated using the plate capacitor capacitance equation

$$C = \varepsilon' \varepsilon_0 S/d, \tag{2}$$

where ε' is the dielectric permittivity of the capacitor insert (nanopowder in our case), C is the measured capacity, d is the dielectric insert thickness, ε_0 is the electric constant, S is the plate area (assuming that in our case the capacitor plates are circular, we get $S = \pi R^2$, where R is the plate radius).

Thus, the resulting equation is written as

$$\varepsilon' = Cd/\varepsilon_0 \pi R^2, \tag{3}$$

where $d = 1$ mm, $\varepsilon_0 = 8.854 \cdot 10^{-12}$ F/m, $\pi = 3.14$, $R = 5$ mm.

We can also estimate the imaginary permittivity component ε'' from the relation for already measured loss-angle tangent.

$$\mathrm{tg}\,\delta = \varepsilon''/\varepsilon'. \tag{4}$$

Thus, the measured temperature dependences of capacity $C(T)$ were used to built the dielectric permittivity dependences $\varepsilon'(T)$ and $\varepsilon''(T)$ (Figure 4).

As shown in Figure 4, ε' and ε'' grow gradually with the temperature rise throughout the temperature dependence. Maximum ε' and ε'' achieve 60 and 45 respectively. Such values are typical for conductors, which is expectable due to the presence of more than 40% of conducting Cu, Zn particles and up to 30% of Cu/Zn composite in the powder. Growth of ε' and ε'' with an increase in temperature is probably associated with the growth of conductivity if metal nanoparticles.

Near 130 K, sharp stepwise growth of $\varepsilon'(T)$ and, accordingly, peak of $\varepsilon''(T)$ are observed. For more detailed study of the anomaly, temperature dependences $\varepsilon''(T)$ were measured at different AC frequencies. The measurement data show that $\varepsilon''(T)$ peak moves into higher temperature region with an increase in frequency (Figure 5). Such behavior is typical for the dielectric relaxation and charge carrier thermal activation. Taking into account sharp rise of elastance above ~ 150 K, conductivity growth and, therefore, prevailing contribution of conductivity to capacity at high temperatures may be suggested. Therefore, we tend to believe that the appearance of the peak on $\varepsilon''(T)$ is associated with thermal activation.

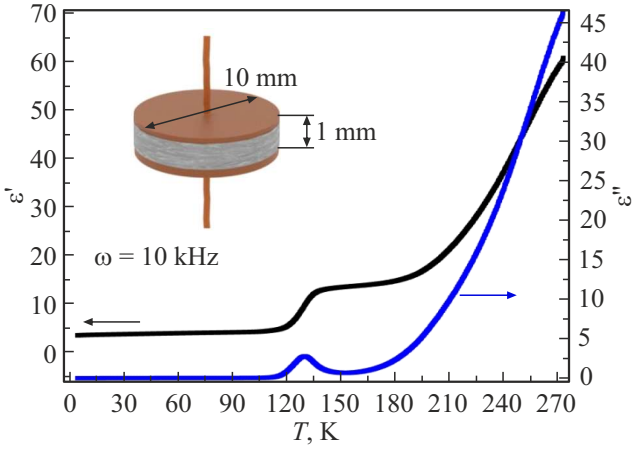

Figure 4. Temperature dependences of the real and imaginary permittivity components ε' and ε'' at AC frequency 10 kHz. Detail — schematic representation of the cell for dielectric powder parameter measurement.

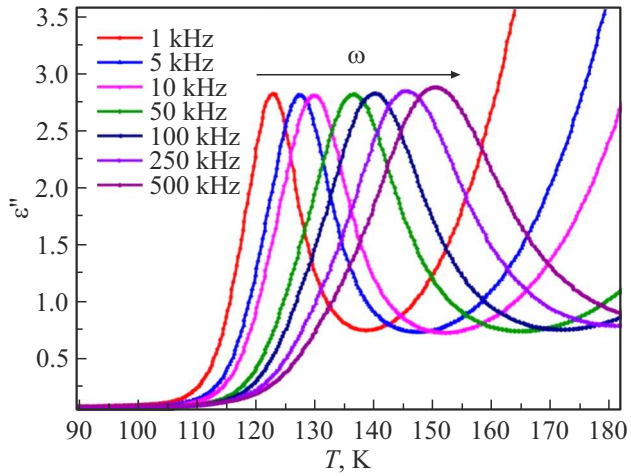

Figure 5. Temperature dependences of the imaginary dielectric permittivity component ε'' at different AC frequencies.

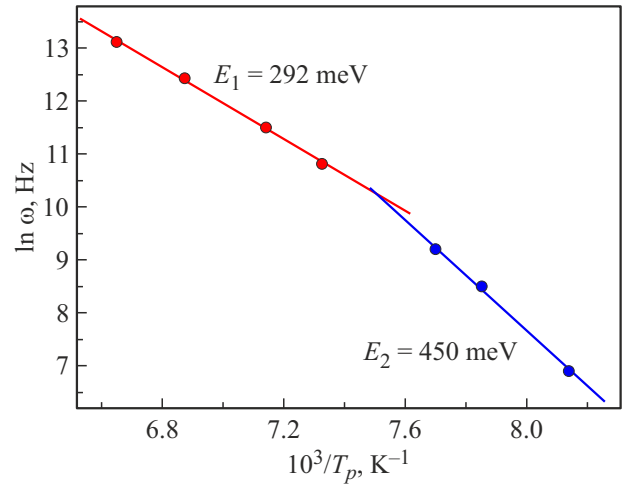

Figure 6. Dependences $\ln\omega$ on the reciprocal temperature of the peak.

Activation energy E may be estimated from the Arrhenius equation:

$$\ln(\omega) = \ln(1/\langle\tau_0\rangle) - E/(k_B T_p), \qquad (5)$$

where T_p is the temperature at which the peak on $\varepsilon''(T)$ is observed at fixed frequency ω, $\langle\tau_0\rangle$ is the mean relaxation time and k_B is the Boltzmann constant.

The energy was estimated using linear approximation of the experimental dependence of $\ln\omega$ on $1/T_p$ and extraction of the approximation line slope (Figgure 6). It can be seen that this dependence is well linearized by two lines resulting in two different activation energies. This may suggest, for example, the presence of two activation processes in two different dielectrics — Cu_2O and ZnO.

Magnetic properties of the sample were investigated using Quantum Design (PPMS-9) system for physical measurements. Measurements were carried out in the temperature range from 5 to 300 K in external magnetic fields up to 90 kOe.

Figure 7 shows the temperature dependence of magnetization measured in the magnetic field of 10 kOe. This dependence demonstrates paramagnetic behavior of the nanoparticles of interest. Since there are no anomalies on the curve that are associated with the long-range magnetic order, then it may be stated that these nanoparticles remain paramagnetic in the temperature range of interest.

Figure 7 shows the temperature dependence of the reverse magnetic susceptibility. It can be seen that it is quite complex. At high temperatures, the obedience to the Curie–Weiss law takes place $\chi = C/(T-\theta)$, where C is the Curie constant, and $\theta = 134$ K is the Curie paramagnetic temperature. Positive sign of the paramagnetic temperature suggests prevalence of ferromagnetic exchange interactions in the system. Comparatively high θ suggests that the Curie–Weiss law is not quite correct for this system Actually, the X-ray diffraction data shows that, in addition to

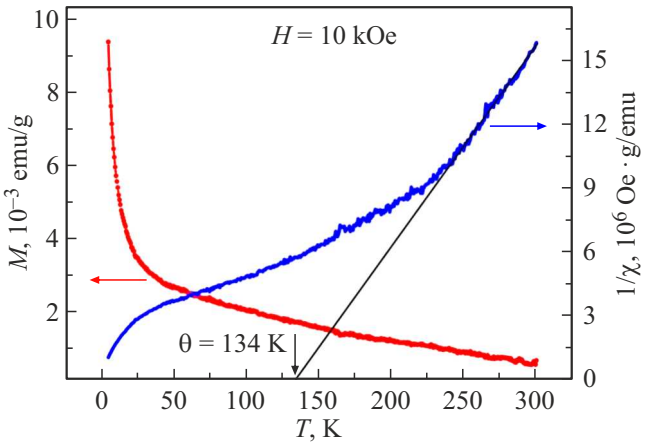

Figure 7. Temperature dependences of magnetization and reverse magnetic susceptibility measured in the field of 10 kOe.

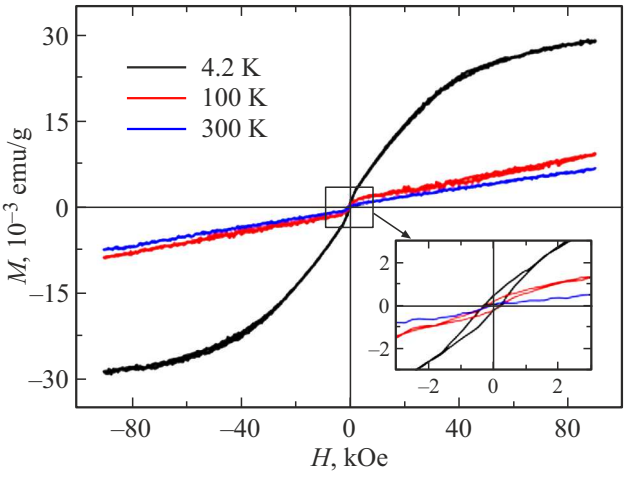

Figure 8. Field dependences of magnetization obtained at different temperatures.

ZnO andCu_2O, the system also contains both metallic and bimetallic particles: Cu, $Cu_{1-x}Zn_x$. Paramagnetic condition of ZnO and Cu_2O may be explained within the Van Vleck paramagnetism orientation model and is well described by the Brillouin function. Whilst the paramagnetic state of Cu, $Cu_{1-x}Zn_x$ may be explained by the paramagnetism of conductivity electrons in metal (Pauli paramagnetism). These two contributions to the magnetic susceptibility explain the complex behavior pattern of $1/\chi(T)$.

Figure 8 shows the field dependences of magnetization at different temperatures. It can e seen that their behavior in the magnetic field is also paramagnetic. It is important that there is a small ferromagnetic phase at the paramagnetic contribution background that can be clearly seen in the detail in Figure 8. This phase is clearly revealed at low temperatures and almost disappears at room temperature. This suggests that some part of composite nanoparticles becomes ferromagnetic. However, the amount of this phase is relatively small, because the temperature dependence of magnetization does not contain any anomalies associated with the established long-range magnetic order. The presence of the ferromagnetic phase is probably associated with the deviation from the Curie–Weiss law at about 250 K (Figure 7) that can be clearly seen on the temperature dependence of the reverse magnetic susceptibility.

4. Conclusion

Composite brass nanoparticles produced by electron-beam evaporation from a two-zone crucible were examined. The nanopowder was subjected to the structural characterization and its composition was measured by the transmission electron microscopy, energy-dispersive X-ray spectroscopy and X-ray diffraction analysis methods. It has been found that the concentration of the declared Cu/Zn nanobrass composite is about 30% of the total mass. The powder does not contain any additional impurities, and the mean particle size is about 120 nm. It can be concluded that this particle production technique is promising, but needs further improvement.

Dielectric properties were studied — temperature dependences of conductivity C(T) were measured at different frequencies and real and imaginary components of the dielectric permittivity (ε' and ε'') were obtained. Near 130 K, a singularity was detected (stepwise growth of $\varepsilon'(T)$ and, accordingly, a peak on $\varepsilon''(T)$), that moved towards higher temperatures with an increase in the AC frequency. Behavior of this singularity is also typical for thermal activation of charge carriers. Is has been shown that the temperature dependence of the peak position on frequency is well described considering two activation energies $E_1 = 292$ and $E_2 = 450$ meV, which is indicative of two different processes, most likely in the Cu_2O and ZnO nanoparticle system.

Investigation of magnetic properties has shown paramagnetic nature of the nanoparticles of interest. Taking into account the chemical analysis of the nanopowder, such result has been anticipated. However, the field dependences of magnetization, besides the paramagnetic contribution, also demonstrate a small ferromagnetic phase. This may suggest that some composite nanoparticles have long-range magnetic order at low temperatures.

Acknowledgments

The authors are grateful to the Krasnoyarsk Regional Collective Use Center of the Federal Research Center, Krasnoyarsk Science Center of the Siberian Branch of the Russian Academy of Sciences, for the provided electron microscopy, X-ray diffraction and magnetic measurement equipment.

Funding

The study was performed within the research theme of the state assignment of Kirensky Institute of Physics, SB RAS.

Conflict of interest

The authors declare that they have no conflict of interest.

References

[1] A.M. Ealias, M.P. Saravanakumar. IOP Conf. Ser.: Mater. Sci. Eng. **263**, 1 (2017).
[2] D.A. Patiño-Ruiz, S.I. Meramo-Hurtado, Á.D. González-Delgado, A. Herrera. ACS Omega **6**, *19*, 12410 (2021).
[3] K.Ch. Sekhar, R. Surakasi, P. Roy, P.J. Rosy, T.K. Sreeja, S. Raja, V.L. Chowdary. Int. J. Chem. Eng. **2022**, 1 (2022).
[4] S.A. Predoi, S.C. Ciobanu, M.C. Chifiriuc, M.M. Heino, D. Predoi, S.L. Iconaru. Materials **16**, *1*, 229 (2023).
[5] U. Asim, N. Shahid, R. Naveed. NANO: Brief Rep. Rev. **7**, *5*, 1 (2012).
[6] P. Luzeau, Z. Xu, M. Lagues, N. Hess, J.P. Coutor, M. Nanto, F. Queyroux, M. Touzeau, D. Pagnon. J. Vac. Sci. Technol. A **8**, *6*, 3938 (1990).
[7] K. Nakaoka, J. Ueyama, K. Ogura. J. Electrochem. Soc. **151**, *10*, 661 (2004).
[8] T. Kimura, Y. Sekio, H. Nakamura, T. Siegrist, A. Ramirez. Nature Mater. **7**, 291 (2008).
[9] T.I. Arbuzova, S.V. Naumov, A.A. Samokhvalov, B.A. Gizhevsky, V.L. Arbuzov, K.V. Shalnov. FTT **43**, *5*, 846 (2001). (in Russian).
[10] S.S.A. Karim, C.F. Dee, B.Y. Majlis, M.A. Mohamed. Sains Malays **48**, *6*, 1301 (2019).
[11] D. Lee, W.K. Bae, I. Park, D.Y. Yoon, S. Lee, C. Lee. Solar Energy Mater. Solar Cells **95**, *1*, 365 (2011).
[12] J. Huang, Y. Wu, C. Gu, M. Zhai, K. Yu, M. Yang, J. Liu. Sens. Actuators B **146**, *1*, 206 (2010).
[13] A.S. Lozhkomoev, O.V. Bakina, A.V. Pervikov, S.O. Kazantsev, E.A. Glazkova. J. Mater. Sci.: Mater. Electron **30**, *14*, 13209 (2019).
[14] M. Sabbouh, A. Nikitina, E. Rogacheva, L. Kraeva, S. Ulasevich, E. Skorb, M. Nosonovsky. Ultrason. Sonochem. **80**, *2073*, 105817 (2021).

[15] E.Ch. Khartaeva, A.V. Nomoev, K.V. Zobov, D.Yu. Trufanov, B.R. Gaponenko, S.P. Bardakhanov. Tr. VII mezhdunar. Kreindelevskogo seminara (2023). S. 189. (in Russian)
[16] Bruker AXS TOPAS V4: General profile and structure analysis software for powder diffraction data. — User's Manual. Bruker AXS, Karlsruhe, Germany (2008).
[17] N.V. Volkov, A.S. Tarasov, D.A. Smolyakov, S.N. Varnakov, S.G. Ovchinnikov. J. Magn. Magn. Mater. **383**, 69 (2015).
[18] D.A. Smolyakov, A.S. Tarasov, I.A. Yakovlev, M.N. Volochaev. Semiconductors. **53**, *14*, 1964 (2019).
[19] D.A. Smolyakov, A.S. Tarasov, M.A. Bondarev, A.A. Nikolskaya, V.K. Vasiliev, M.N. Volochaev, N.V. Volkov. Mater. Sci. Semicond. Proc. **126**, 1 (2021).

Translated by E.Ilinskaya